JOURNAL OF MATERIALS SCIENCE 27 (1992) 3502–3510

General method for determination of crack-interface bridging stresses

XIAO-ZHI HU, YIU-WING MAI
Centre for Advanced Materials Technology, Department of Mechanical Engineering, University of Sydney, NSW 2006, Australia

A simple compliance approach is presented for the determination of crack-interface bridging stresses in *quasi*-brittle materials. This technique is based upon the consideration that an unloading compliance measured experimentally differs from the linear elastic compliance of the same crack length because of the influence of the bridging stresses. A general crack-interface bridging theory is developed from which the bridging stresses can be obtained utilizing the difference in these compliances. Experimental data from a range of engineering materials including alumina and duplex ceramics, cellulose fibre cements and carbon fibre/epoxy composites are used to verify the bridging theory and several interesting results are obtained. A novel toughness curve obtained with a new compliance ϕ function is presented and used to elucidate the crack-interface bridging associated R curve behaviour.

1. Introduction

The concept of crack resistance, R, curve has been frequently used to characterize the crack growth resistance, in terms of either the stress intensity factor, K_R, or the potential energy release rate, G_R, with crack extension, Δa, for a wide range of engineering materials including many fibre composites, ceramics and cementitious materials [1–4]. One of us [2] has recently discussed the various types of toughening mechanisms associated with these different materials that would give rise to crack-tip shielding so that the fracture toughness is apparently increased. For convenience, these toughening mechanisms can be broadly divided into two categories: frontal shielding (ahead of the crack tip) and wake shielding (behind the crack tip). Examples of the former are plasticity-induced toughening, frontal microcracking, crack front deflection and twisting etc.; examples of the latter are notably phase transformation toughening, fibre and grain bridging.

In this paper we are primarily concerned with the wake shielding or crack-interface bridging mechanisms that produce the crack resistance curves which have already been reported for several materials, e.g. fibre composites [5–7], ceramics [8–10] and cementitious materials [11–13]. Here, bridging is used to mean that the crack-interface behind its advancing tip is still connected, either by unbroken fibres (for fibre composites) or by localized grain interlocking, zig-zagging and branching cracks leaving behind untorn ligaments (for ceramics and cementitious materials). Consequently, bridging stresses represent any cohesive (or closure) stresses behind the crack tip, which are generated by fibre or grain pull-out and any other damage processes in the bridging zone. It is these bridging stresses that effectively shield the crack tip and hence are responsible for the rising crack resistance curve behaviour of these materials. Thus, if the bridging stresses can be accurately measured, toughness characterization and theoretical modelling of R curves may be very easily conducted. Despite some attempts to measure such stresses using both direct [14, 15] and indirect [16–18] methods, they are either too difficult experimentally or the results too subjectively interpreted. Besides, all these measurements have been exclusively restricted to cementitious materials. The purpose of this paper is to establish a general method which can be easily used to determine the bridging stresses in any given material that has a R curve characteristic due to crack shielding mechanisms operating at the wake of the crack tip.

The classic crack-wake sawcut experiments of Knehans and Steinbrech [8] have provided some direct evidence for the influence of crack-interface bridging in alumina ceramics by comparing the two R curves obtained before and after the sawcut. The R curve of an alumina notched-bend specimen was first measured for a certain amount of crack growth. Then the specimen was re-notched nearly to the observed crack tip and the R curve remeasured. It was found that at the beginning the R curve obtained after re-notching did not follow the previous R curve before re-notching. Instead it started at a lower value and only resumed the trend of the previous R curve after some crack growth. These results can only be satisfactorily explained in terms of the removal of bridges due to re-notching and they demonstrate the unequivocal influence of the bridging stresses on the R

0022–2461

curve behaviour of alumina ceramics. However, Knehans and Steinbrech did not show how to determine quantitatively these bridging stresses behind the crack tip.

A consecutive sawcut experiment in conjunction with compliance measurements, recently introduced by Hu and Wittmann [13, 19–21], has been designed to overcome this shortcoming. In their method, an amount of crack extension was generated in a specimen by application of an external load so that a fully bridged crack was developed. The specimen then underwent a series of sawcuts along the propagated crack so that each time a small portion of the fully developed bridging zone was removed. Compliance measurements corresponding to the removal of bridges at particular sites were then determined and used to calculate the bridging stresses [13, 20, 21]. Basically, the theory relates the compliance measurements to the influence of the bridging stresses. This theory was further verified with computer simulation experiments [22] on compact tension (CT) specimens made from two different mortars. From the bridging stresses determined in the consecutive cutting experiments, complete load/displacement curves of the specimens and compliance variations during cutting were simulated. These results compared well with the actual experimental data.

It is believed that the consecutive cutting technique is suitable to cementitious materials, coarse grain ceramics with long bridging zones, continuous fibre composites with a crack propagating transversely to the fibres, and short fibre reinforced composites. However, this technique may not be applied to certain ceramic materials for which bridging zones developed are too small due to either limited specimen size or their fine grain structures. It is also difficult to conduct cutting experiments on mode-I interlaminar delamination of polymer fibre-composites although the fibre bridging zones may be quite large. In this case, bridging is mainly due to the misalignment of fibres between individual plies within one laminate and fibre bridging occurs across the crack surfaces at different sites. Therefore, any cutting along the delamination plane will not only remove local bridges but also alter remote bridges linked by the same fibres. In the present paper, we seek to extend the original bridging stress theory developed by Hu and Wittmann [13, 20, 21] so that the bridging stresses can be determined without any consecutive sawcuts. Experimental results from a range of materials are used to verify the extended theoretical model and these include carbon fibre/epoxy composites [23] with and without a polyvinyl alcohol (PVAL) coating, cellulose fibre cements tested in both dry and wet conditions [5], an alumina [24] and a deplex ceramic [25, 26].

2. Theoretical basis

Compliance is one of the most common measurements that can be made in a fracture propagation experiment. Unloading of a specimen during testing to determine the compliance, C_u, is now an accepted method to measure the propagated length of a crack. However, if crack-interface bridging develops behind a crack tip due to crack shielding mechanisms discussed in the last section, for such materials as fibre composites, coarse grain aluminas and cementitious materials, the compliances, C_u, measured upon unloading after some crack propagation are inevitably reduced by the bridging stresses closing up the crack. Thus, the crack length cannot be accurately inferred from these C_u measurements. We present in this section an extension of the compliance and bridging stress theory by Hu and Wittmann [13, 20, 21] so that we can determine bridging stresses simply from the compliance measurements, C_u, with no consecutive sawcutting. This extended theory, therefore, has a broader application since the limitation in performing a sawcut experiment has been removed and compliance measurements with and without bridging influence can be easily obtained.

A general bridging stress/crack face opening, σ_b/ω, relationship is shown schematically in Fig. 1a for

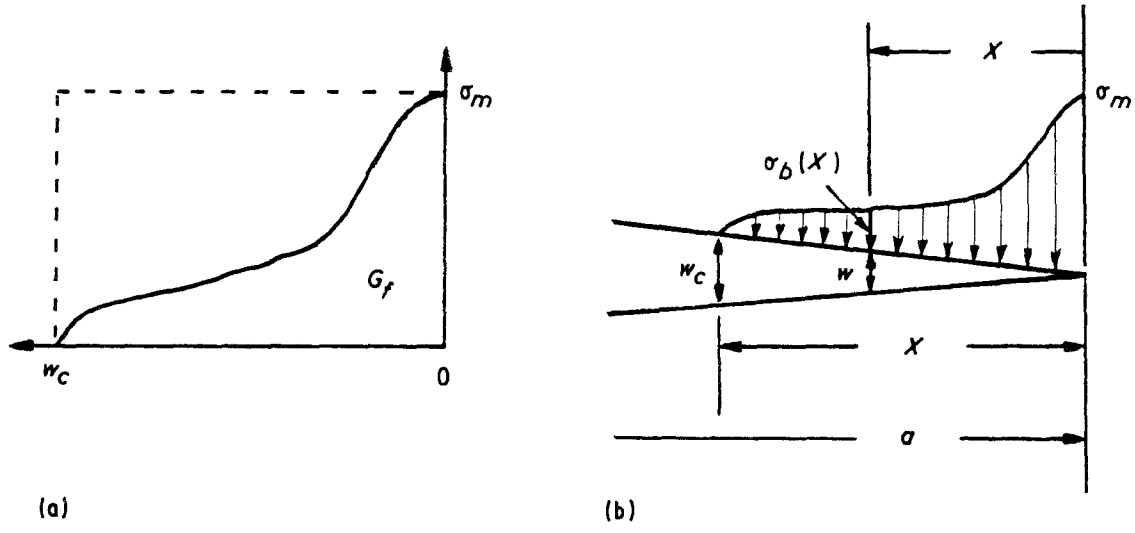

Figure 1 (a) Bridging stress crack opening ($\sigma_b - \omega$) relationship of strain-softening materials; (b) crack-interface bridging stresses within the bridging zone, X, are controlled by the $\sigma_b - \omega$ relationship.

strain-softening materials. Here, softening implies that the bridging stress, σ_b, decreases monotonically with crack face opening displacement, ω. The most important material properties are: the maximum bridging stress σ_m (or the tensile strength of material [11]), the specific fracture energy, G_f, which is the area under the σ_b–ω curve, the critical crack face opening displacement, ω_c, when the bridging stress becomes zero, and the shape of the bridging stress distribution curve.

A graphical representation of a fully saturated bridging zone, X, is shown in Fig. 1b. Let $C(a)$ be the compliance of a specimen with a crack length, a, with no bridging and C_u the compliance measured in an experiment for the same a but with the influence of bridging stresses. $C(a)$ can be either calculated theoretically or measured experimentally. It is expected that

$$C(a) > C_u \tag{1}$$

since bridging stresses behind the crack tip reduce the compliance. Hence, the crack length is underestimated if the conventional compliance method is used indiscriminately because the compliance only corresponds to some effective crack length a_{eff}, i.e. $C_u = C(a_{eff})$, and $a_{eff} < a$.

Consider now Inequality 1 with respect to a sawcut experiment. If a sawcut is extended right to the crack tip, C_u thereafter determined is the same as $C(a)$. If a series of sawcuts are now performed to remove the bridging zone (shown in Fig. 1b) in a step-wise fashion and the corresponding compliances C_u determined after each sawcut, Inequality 1 eventually becomes an equality as the bridging influence on C_u values is gradually diminished to zero. To illustrate the working principle of this concept we consider a consecutive cutting experiment on a CT specimen of cement mortar as shown in Fig. 2. The x axis, Δa, indicates the increment of the sawcut notch length from the tip of the initial notch taken as the origin. That is $\Delta a = a - a_0$, where a_0 is the initial notch length. $C_u(\Delta a)$ is virtually unchanged even after the notch length has been increased up to 32 mm by 6 successive sawcuts since no bridges are removed. $C_u(\Delta a)$ begins to increase as soon as some bridging stresses have been removed by cutting. Values of $C_u(\Delta a)$ within the bridging zone has been fitted with a solid curve and compared with the compliance calibration curve for specimens with traction-free cracks. In this case, the initial compliance ratio before cutting $C_u/C(a) \approx 0.6$, which verifies the Inequality 1. Fig. 2 also gives the additional information that the bridging zone length, X, is about 34 mm and that if C_u is used to determine the crack length it is underestimated by about 10 mm.

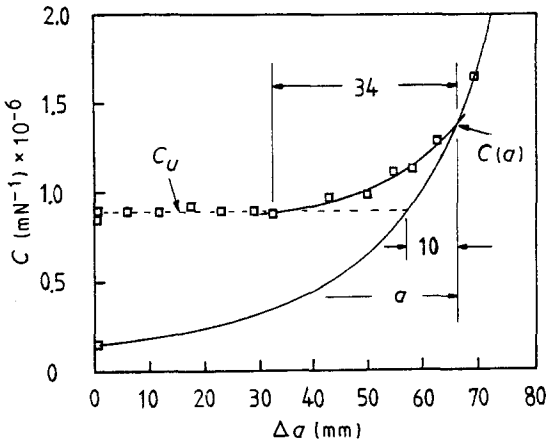

Figure 2 Consecutive sawcutting results from a mortar CT specimen: the bridging zone $X = 34$ mm, the effective crack from C_u underestimates the crack a by 10 mm, C_u curve within the bridging zone, X, is directly related to the bridging stress distribution [20, 21].

If $\omega_c/X \ll 1$, as in most brittle materials, a linear crack face profile can be assumed within the bridging zone (see Fig. 1b), i.e.

$$\frac{\omega}{\omega_c} = \frac{x}{X} \tag{2}$$

Based on this assumption, a general theory has been developed to convert the variation in C_u into the bridging stress σ_b at the site where the sawcut took place [13, 20, 21]. It is proved that during the consecutive cutting

$$\frac{\sigma_b(x)}{\sigma_m} = -\frac{C^2(a)}{C'(a)}\frac{C'_u(x)}{C_u^2(x)} \tag{3}$$

where $C'(a) = dC(a)/da$ and $C'_u(x) = dC_u(x)/dx$, and that before any sawcut (see Fig. 1b)

$$\frac{C(a)}{C'(a)}\left\{\frac{C(a)}{C_u} - 1\right\} = X\frac{G_f}{\sigma_m\omega_c} \tag{4}$$

Obviously, Equation 4 is valid for any C_u measurement after the full bridging zone has been developed and it represents the compliance measurement without any sawcut. Note that in Equation 3, however, $C_u(x)$ is used for the compliance measurement after the sawcut is made to a distance, x, away from the crack tip (Fig. 1b).

To extend this theory for the evaluation of bridging stresses without introducing sawcuts to the bridged crack we realize that an unsaturated bridging zone is identical to a bridging zone which has been fully developed and then partially removed by sawcutting. Therefore, Equation 3 can also be used to analyse the compliance C_u before a bridging zone is fully developed. Let σ_T indicate the bridging stress at the initial notch tip and C_u the measured compliance before the bridging zone is fully developed. Equation 3 hence becomes

$$\frac{\sigma_T}{\sigma_m} = \frac{\sigma_b(x)}{\sigma_m} = -\frac{C^2(a)}{C'(a)}\frac{C'_u}{C_u^2} \quad \Delta a < X \tag{5}$$

where $C'_u = dC_u/dx$ as before. During unloading only C_u, rather than $C'_u(= dC_u/dx)$, is measured. Therefore, Equation 5 needs to be further modified.

Foote *et al*, [12] proposed a simple power law relationship for bridging stresses in strain-softening materials

$$\frac{\sigma_b}{\sigma_m} = \left[1 - \frac{\omega}{\omega_c}\right]^n \quad n > 0 \tag{6}$$

The softening index or exponent n depends on the precise bridging mechanisms. For instance, $n = 1$ is typical of materials where frictional pull-out is the

major toughening mechanism. The specific fracture energy, G_f, dissipated in the bridging zone is given by

$$G_f = \int_0^{\omega_c} \sigma_b d\omega = \frac{\sigma_m \omega_c}{n+1} \quad (7)$$

using Equation 6 for σ_b. Therefore, the softening index n is well defined by G_f, σ_m and ω_c. From Equation 7 and Fig. 1a, it is clear that $1/(n+1)$ is simply the ratio of the energies $G_f/\sigma_m\omega_c$, or the areas under the solid and dash lines in Fig. 1a. This ratio is what can be determined by experiment through Equation 4. It is clear that for strain-softening materials $G_f/\sigma_m\omega_c < 1$. This relationship holds for most quasi-brittle materials.

Equation 6 simplifies the application of Equation 3 or 5 in the case where a bridging zone has not been fully developed. By substituting Equations 2 and 6 into Equation 3 or 5, it is obtained that

$$-\frac{C^2(a)}{C'(a)}\frac{dC_u(x)}{C_u^2(x)} = \left[1 - \frac{x}{X}\right]^n dx \quad (8)$$

Integrating this equation for $0 < x < \Delta a$ and $C(a) > C_u(x) > C_u$, we obtain

$$\frac{C(a)}{C'(a)}\left\{\frac{C(a)}{C_u} - 1\right\} = \frac{X}{n+1}\left\{1 - \left[1 - \frac{\Delta a}{X}\right]^{n+1}\right\} \quad (9)$$

where C_u is simply the compliance before the bridging zone is fully developed. It can be seen by comparison of Equations 4 and 9 that the left hand sides of both equations denoted by ϕ below are exactly the same whether the bridging zone is fully developed or not. Hence

$$\phi = \frac{C(a)}{C'(a)}\left\{\frac{C(a)}{C_u} - 1\right\} = \begin{cases} \frac{X}{n+1} & \Delta a \geq X \\ \frac{X}{n+1}\left\{1 - \left[1 - \frac{\Delta a}{X}\right]^{n+1}\right\} & \Delta a < X \end{cases} \quad (10)$$

If $\Delta a/X \ll 1$, the above equation can be simplified to

$$\phi \approx \Delta a \quad (11)$$

It is also interesting to look at the derivative $d\phi/da$ (for $\Delta a < X$) given by

$$\frac{d\phi}{da} = \left[1 - \frac{\Delta a}{X}\right]^n = \left[1 - \frac{\omega}{\omega_c}\right]^n = \frac{\sigma_b}{\sigma_m} = \frac{\sigma_T}{\sigma_m} \quad (12)$$

if X is constant and $da = d(a_0 + \Delta a) = d\Delta a$. However, it should be emphasized that before a bridging zone is fully developed, X only indicates the distance from the crack tip to a point where the crack face opening is equal to ω_c. Therefore, X may well be a variable depending on geometry and size etc. and the application of Equation 12 to determine bridging stresses is restricted.

Let G_i and K_i be the initial values of G_R and K_R curves, and G_∞ and K_∞ be the plateau values. G_f or the area under the $\sigma_b - \omega$ softening curve can also be given by [2, 4]

$$G_f = G_\infty - G_i = \frac{1}{E}[K_\infty^2 - K_i^2] \quad (13)$$

where E is the Young's modulus. Hence, G_f in Equation 7 can be determined from crack-resistance curves.

If both crack growth, Δa, and compliance, C_u, are measured experimentally, a ϕ curve can be constructed using Equation 10. From the ϕ curve both the fully saturated bridging zone, X, and the softening index, n, can be easily determined. Since $1/(n+1)$ is the energy ratio $G_f/\sigma_m\omega_c$ as given by Equation 7, the ϕ curve is actually a material toughness curve.

It is also worth noting that during the consecutive sawcut experiments shown in Fig. 2 the crack length, a, remains constant; only the fully saturated bridging zone, X, is removed in a step-wise fashion by an amount dx. Differentiating ϕ with respect to x and keeping a constant gives

$$\frac{d\phi}{dx} = -\frac{C^2(a)}{C'(a)}\frac{C_u'(x)}{C_u^2(x)} = \frac{\sigma_b(x)}{\sigma_m} \quad (14)$$

which is Equation 3 used for the derivation of Equation 10.

The compliance form of Equation 10 can be used to determine $\phi(a)$ in Equations 12 and $\phi(x)$ in Equation 14. $\phi(a)$ in Equation 12 is measured as a function of the crack length, a, and no sawcut is involved in its evaluation. On the other hand, $\phi(x)$ in Equation 14 is measured during consecutive cutting, and the crack length, a, remains constant. However, in both situations the function ϕ defined by the compliance form of Equation 10 does provide a simple solution for the evaluation of bridging stresses. The fact that ϕ can be easily measured in experiment makes the method more attractive.

3. Bridging stresses in ceramic materials

3.1. K_R and ϕ curves of an alumina

The R curve behaviour in alumina has been studied by many authors. Probably the work of Swanson *et al.* [27] provides the most convincing evidence on crack-interface grain bridging behind the tip of a crack. The evolution of localized grain bridges in a coarse grain alumina can be clearly seen from their *in-situ* micrographs. The two R curves obtained by Knehans and Steinbrech [8] from their crack wake sawcut experiments also demonstrate the bridging effect on the fracture resistances of alumina before and after the sawcut. Thus alumina is an ideal material to apply the bridging stress theory summarized in Equation 10.

In the work of Lathabai *et al.* [28], a coarse grain alumina (35 μm) was tested in a CT specimen with an initial a_0/W ratio of 0.325 where a_0 was 14.28 mm and the thickness, t was 2 mm. Both crack length, a, and corresponding compliance, C_u, were measured in their experiments. These data are used to construct the K_R and ϕ curves shown in Fig. 3. Standard formulae for CT specimens are used to calculate the stress intensity factor, K, and the compliance $C(a)$ without crack-interface bridging.

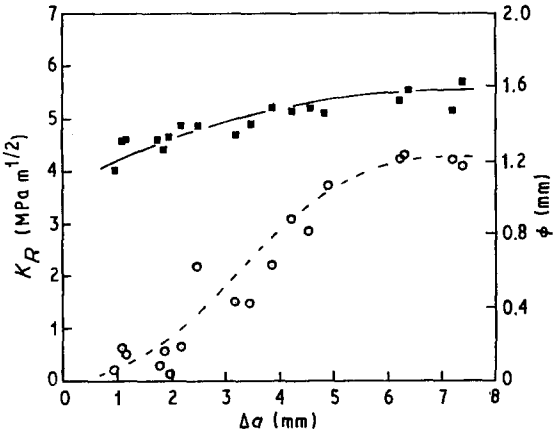

Figure 3 Crack resistance curve of an alumina (35 μm) measured with a CT specimen [28], and the corresponding ϕ curve: (■) K curve and (○) ϕ curve.

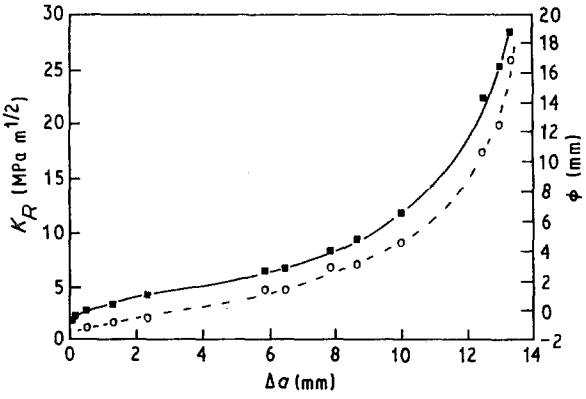

Figure 4 Crack resistance curve of a duplex ceramic measured with a CT specimen [25, 26], and the corresponding ϕ curve (■) K curve and (○) ϕ curve.

From the K_R curve in Fig. 3 it appears that when crack growth commenced there was a rapid crack extension of about 1 mm although the specimen had been pre-cracked from the sawcut notch. It is therefore not easy to define K_i from this K_R curve but the plateau value, K_∞ (≈ 5.5 MPa m$^{1/2}$) is clearly observed when the crack extension, Δa, is bigger than 5 mm. The ϕ curve in the same figure shows a steady increase of ϕ with Δa until its plateau value, ϕ_∞, of 1.2 mm is reached for $\Delta a > 5$ mm. By comparison of the first few data points in Fig. 3 and Equation 11 (i.e. $\Delta a \ll X$) it can be concluded that crack bridging has not been established until Δa is about 1 mm from the initial notch tip. The initial rapid crack extension of nearly 1 mm also supports this conclusion. Therefore, the fully saturated bridging zone, X, should be between 4 to 5 mm, rather than 5 to 6 mm as shown in Fig. 3. Due to the scatter in ϕ over the region of $1 < \Delta a < 5$, it is impracticable to apply Equation 12 to determine the bridging stress distribution. However, the relationship that $\phi_\infty = X/(n+1)$ for $\Delta a > X$ provides a simple solution to evaluate n and the bridging stresses. Assuming the average $X = 4.5$ mm and since $\phi_\infty = 1.2$ mm, we obtain $n = 2.8$.

3.2. K_R and ϕ curves of duplex ceramic

Mechanical properties and K_R curve behaviours of duplex ceramics have been studied extensively by Lutz and his co-workers [25, 26, 29]. The duplex ceramic is a two phase material based on alumina and zirconia. The well dispersed second phase particles form the pressure zones due to their volume expansion associated with phase transformation upon cooling from the fabrication temperature. These particles or pressure zones cause crack deflection and branching or chained cracks ahead of the main crack giving rise to an effectively reduced elastic modulus of the local material. This is equivalent to a frontal microcracking zone. As the main crack is extended these pressure zones together with the untorn ligaments of the chained cracks induce a closure stress at the wake of the crack tip. Consequently, the crack growth resistance of the duplex ceramic is increased. Equation 10 therefore can be used in this case to determine the equivalent bridging stresses at the crack-interface.

One of the K_R curves of a duplex ceramic [25] is shown in Fig. 4, which is measured using a CT specimen with dimensions $26 \times 23 \times 3$ mm^3, and an initial ligament ($W - a$) of 15 mm (see experimental details in References 25 and 26). The corresponding ϕ curve is evaluated with Equation 10 using the compliance data [30].

It is not possible to determine the fully saturated bridging zone, X, from either the K_R or ϕ curve of the duplex ceramic without a critical examination of these toughness curves because X is so large that both resistance curves are affected by the end effects of the specimen geometry as the bridging zone approaches the boundary of the specimen. These end effects on R curves have been discussed recently [3, 4, 31].

Equation 10 indicates that ϕ should always be less than Δa for strain-softening materials since $n > 0$. However, ϕ starts with -2 and the last three measurements of ϕ in Fig. 4 indicate that $\phi + 2 > \Delta a$. Hence, the toughness curves for $\Delta a > 10$ mm should not be considered as true material properties. If the plateau value for the duplex ceramic is reached at Δa between 8 and 10 mm, K_∞ is between 9 and 13 MPa m$^{-1/2}$ as reported in [30]. Then $X/(n+1) = \phi_\infty + 2$ and $n = 0.6$–0.5. The upper and lower bounds of K_∞, estimated in this way for the duplex ceramic are comparable to K_∞ of 7 and 9 MPa m$^{-1/2}$ of two similar duplex ceramics [25].

The reason that ϕ starts with a negative value is because Equation 10 considers only crack-interface bridging. If the amount of microcracking in the frontal process zone of the main crack is small compared to crack wake bridging such as in aluminas, ϕ is greater than zero. However, if extensive microcracking occurs such as in this duplex ceramic with multiple chained cracks before the growth of the main crack, the stiffness of the material is reduced and ϕ starts with a negative value.

4. Bridging stresses in fibre composites

4.1. K_R and ϕ curves of cellulose fibre cements

R curve behaviours of cellulose cements under both

wet and dry conditions have been investigated by Mai and Hakeem [5] using double cantilever beams (DCB) with an initial crack length of 37 mm, specimen thickness 5 mm and width 70 mm. The elastic moduli of the cellulose fibre cements are: 5.50 and 9.65 GPa, respectively, for wet and dry conditions. Crack resistance curves are given in Fig. 5 in which the G_R curves are obtained using linear elastic fracture analysis and the modified potential energy release rate G_R^* curves are constructed by taking into account the residual displacement at zero load [5].

The difference in compliances for a traction-free notch and a bridged crack of the same length has been emphasized and demonstrated with experimental results. They found for the same crack length the compliance for the traction-free notch was bigger than that for the natural crack because of fibre bridging. Therefore, the ϕ curve approach given in Equation 10 should apply. Using their compliance data for both the wet and dry DCB cellulose fibre cements, corresponding ϕ curves are obtained in Fig. 6.

From Figs 5 or 6 it can be estimated that the fully saturated bridging zone $X \approx 50$ mm for both wet and dry conditions. However, Fig. 6 shows that $\phi_\infty \approx$ 21 mm for wet and ≈ 11 mm for dry conditions. The scatter in the plateau region of ϕ in Fig. 6 suggests that the fracture propagation of cellulose fibre cements in dry condition is not as stable as tested in wet. From Equation 10 ($n = X/\phi_\infty - 1$) we obtain $n = 1.4$ and 3.5 for wet and dry conditions. Since a bigger softening index n means that the bridging stress decreases more quickly away from the crack tip and that fracture is less stable, these wet and dry values of n are consistent with the G_R curves shown in Fig. 5.

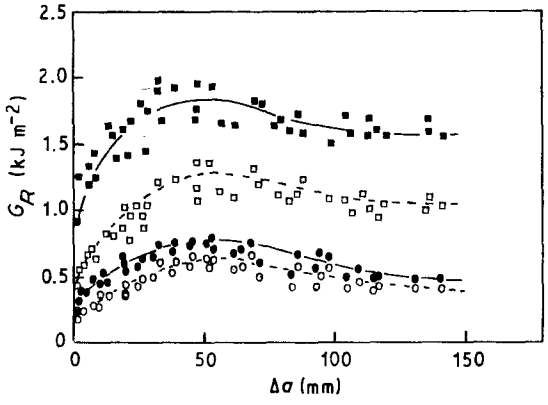

Figure 5 Crack resistance curves of cellulose fibre cements measured with DCB specimens [5]: (■) G_R^* (wet); (□) G_R (wet); (●) G_R^* (dry) and (○) G_R (dry).

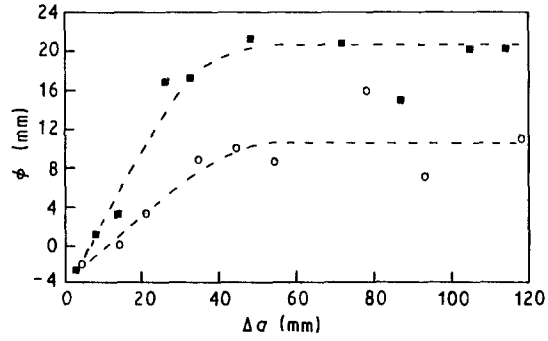

Figure 6 ϕ curves of two cellulose cement specimens tested under the wet and dry conditions: (■) wet and (○) dry.

4.2. K_R and ϕ curves of carbon fibre/epoxy composites

It is well-known that the fracture toughness of a fibre/polymer composite is not simply the sum of contributions by the constituents, but is governed more importantly by the extent of energy absorption processes through various toughening mechanisms, depending on fibre and matrix properties, and the nature of bonding at the fibre/matrix interface. The effects of an interfacial coating of polyvinyl alcohol (PVAL) on Charpy impact and mixed mode fracture toughnesses of unidirectional carbon fibre reinforced epoxy resin composites have been investigated by Kim and Mai [32, 33]. The mode-I delamination fracture toughness of the same carbon fibre/epoxy composites with and without a PVAL coating on the fibres has also been studied [23] using DCB specimens, approximately $20 \times 3.7 \times 150$ mm^3, made up from 12-ply unidirectional carbon fibre/epoxy composites. Pre-cracks 36 to 40 mm in length were introduced in the midplane of the thickness with Teflon tapes. The compliances were measured as a function of delamination crack growth by successive loading and unloading of the specimen. Using these data the K_R and ϕ curves for the two types of composites were determined. Example K_R and ϕ curves are given in Fig. 7 for the uncoated fibre composite, and Fig. 8 for the coated fibre composite.

It was observed that the fibres bridging across two crack surfaces often form a bundle. The failure or even partial failure of the bundle of bridging fibres causes local unstable fractures as shown by the discontinuous curves in Fig. 7. This characteristic was observed for both coated and uncoated fibre composites. However, delamination was over-all more stable for the PVAL coated composite due to the presence of a rubbery coating on the fibres. Since the composites were made up from unidirectional fibres and the pre-crack was introduced between two plies, fibre bridging might not always be established at the beginning of delamination as shown in Fig. 8.

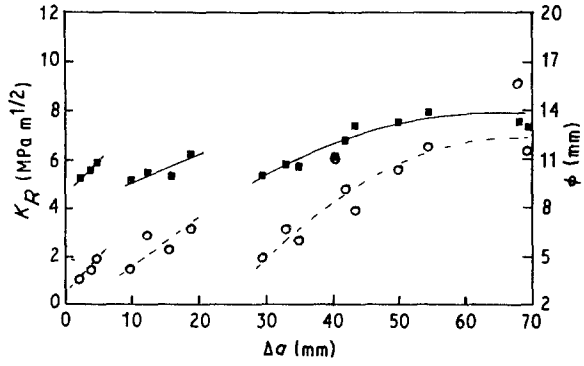

Figure 7 Mode-I delamination resistance curve of carbon fibre/epoxy composite measured with a DCB specimen [23], and the corresponding ϕ curve: (■) K curve and (○) ϕ curve.

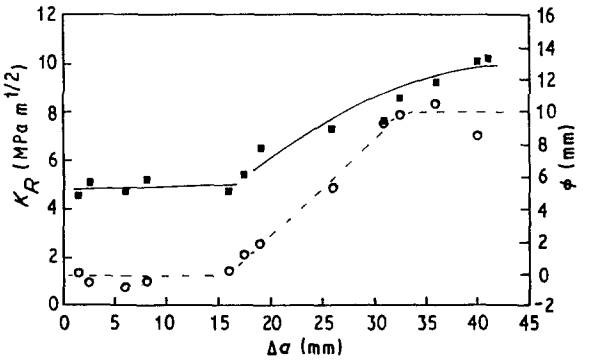

Figure 8 Mode-I delamination resistance curve of polyvinyl alcohol (PVAL) coated carbon fibre/epoxy composite measured with a DCB specimen [23], and the corresponding ϕ curve: (■) K curve and (○) ϕ curve.

The ϕ-curve in Fig. 8 for Δa between 0 and 17 mm shows that $\phi = 0$ thus supporting the observation that no fibre bridging exists in this region. However, ϕ rises with Δa for longer delamination crack growth confirms that the dominant toughening mechanism for the R curve behaviour is due to fibre bridging behind the crack tip.

Taking all the K_R and ϕ curves together we obtain $K_\infty = 10$ MPa m$^{1/2}$ and $\phi_\infty = 9.4$ mm for the PVAL coated composite, and $K_\infty = 8$ MPa m$^{-1/2}$ and $\phi_\infty = 11$ mm for the uncoated composite. The fully saturated fibre bridging zone, X, is about 25 to 30 mm for the PVAL coated fibre composite and 30 to 35 mm for the uncoated fibre composite. However, the softening index $n \approx 2$ for both cases.

5. Discussion

5.1. Bridging stress distribution

The softening index, n, in Equation 6 defines the non-dimensional bridging stress distribution, σ_b/σ_m versus ω/ω_c. Equation 10 has so far been applied to various materials to determine n. One common feature clearly shown in Figs 3–8 is that both the K_R (or G_R) and ϕ curves of any given material are very similar graphically. They reach the plateau values at the same crack extension (e.g. Fig. 3 for the alumina); show similar increasing trends with Δa (e.g., Fig. 4 for the duplex ceramic); give higher plateau values for wet cellulose fibre cements (Figs 5 and 6); display the same localized unstable delamination crack growth of the uncoated carbon fibre/epoxy composite (Fig. 7); and prove that crack-interface bridging is the major toughening mechanism in the PVAL coated carbon fibre/epoxy composite (e.g. Fig. 8 shows that K_R is constant at about 5 MPa m$^{1/2}$ and $\phi = 0$ if no bridging exists and when bridging takes effect both K_R and ϕ rises with Δa).

The softening index, n, of alumina ceramics determined with other methods are recently reported in the literature. For instance, $n \approx 2.5$ has been obtained from *in-situ* scanning electron microscope (SEM) measurements of the crack profile behind a crack tip for an alumina with an average grain size of 11 μm [34]; and $n \approx 3$ determined from R curve fitting by trial and error [31] for an alumina with an average grain size of 16 μm. These n values compare very well with our result of $n = 2.8$ and this agreement lends some support to the bridging stress theory developed in this paper. However, the compliance-based method is much simpler to perform than the others.

Besides the determination of the non-dimensional bridging stress distribution (σ_b/σ_m versus ω/ω_c), a ϕ curve may also be used to verify whether crack surface bridging is the major toughening mechanism (i.e. $\phi > 0$) as shown in Fig. 8, and whether a K_R curve is still valid (i.e. $\phi < \Delta a$) as shown in Fig. 4.

5.2. Crack wake bridging and frontal microcracking

According to Equation 10, ϕ should be always bigger than, or at least equal to zero. However, it is noticed that sometimes a ϕ curve starts with a negative value, such as in Figs 4 and 6. This phenomenon can be explained with limited frontal microcracking before the propagation of a main crack.

If microcracking exists before any visible crack extension the experimental compliance, C_u, of a specimen will be increased due to the damage in front of the initial crack a_0. Since $C(a_0)$ is the compliance without any damage and bridging it follows that:

$$C(a_0) < C_u \tag{15}$$

Thus ϕ evaluated with Equation 10 will be less than zero. Let us now assume that both microcracking and bridging mechanisms coexist in a material. A ϕ curve defined by Equation 10 will start with a negative value, and gradually increase with crack extension when bridging is developed behind the crack tip. When contributions to the compliance from microcracking and bridging are balanced after a certain amount of crack extension, $\phi = 0$. If crack-interface bridging is the main toughening mechanism, ϕ will be bigger than zero with further increase in crack growth. Normally if a microcracking mechanism exists in a material, microcracks will always be generated in front of the advancing main crack. This influence in toughness throughout the crack growth process can be estimated by the initial negative ϕ value, as is done for the duplex ceramic (i.e. $\phi + 2$ is used for the toughness evaluation).

From the above discussion and Inequalities 1 and 15, it is clear that a ϕ curve can be used to estimate the relative influence of crack-interface bridging and frontal microcracking. Therefore, it can be argued from the ϕ curves shown in Fig. 6 that microcrack toughening compared with fibre bridging is negligible in cellulose fibre cements tested in both wet and dry conditions. However, if both the K_R and ϕ curves in Fig. 4 are valid only for $\Delta a < 10$ mm, microcracking may contribute a quarter of the total toughness increase of the duplex ceramic although the crack-interface bridging is still the major toughening mechanism (i.e. at $\Delta a = 10$ mm ϕ from bridging is about 6 since ϕ from microcracking is around 2). Extensive microcracking observed in the duplex ceramic specimens using a special dyeing technique [25] confirms this conclusion deduced from the ϕ curve in Fig. 4.

5.3. Frictional degradation analysis with ϕ function

One useful extension of the ϕ curve approach is in cyclic fatigue of quasi-brittle materials with crack-interface bridging as the main toughening mechanism such as in aluminas. The complex fatigue crack growth process is inevitably influenced by the R curve behaviour from bridging while bridges developed behind the crack tip are subjected to frictional degradation due to cyclic loading. This coupling problem cannot be solved by simply superimposing the R-curve behaviour onto the cyclic crack growth law. The friction degradation of bridges has to be known explicitly before the R curve behaviour can be incorporated in a cyclic fatigue analysis.

Consider a fully saturated bridging zone, X. During cyclic fatigue, the frictional degradation of bridges can be evaluated by the compliance ϕ function if the fatigue crack growth of the main crack, a, can be suppressed, or limited when compared with X. This requires the maximum cyclic load should be always less than the critical load at which the main crack, a, grows during fatigue. Let N indicate the number of fatigue cycles. Under the condition that a is approximately constant, only the unloading compliance, C_u, in the ϕ function is influenced by the frictional degradation of the bridges. From Equations 4 and 10

$$\begin{aligned}\phi(N) &= \frac{C(a)}{C'(a)}\left\{\frac{C(a)}{C_u(N)} - 1\right\} \\ &= \frac{G_f(N)}{\sigma_m \omega_c(N)} X(N) \\ &= \frac{1}{n+1} X(N) \end{aligned} \tag{16}$$

where a is a constant. The frictional degradation reduces the magnitude of the bridging stress $\sigma_b(N)$, the critical crack opening $\omega_c(N)$, and then $G_f(N)$ the area under the $\sigma_b(N)$–$\omega_c(N)$ curve, as shown in Fig. 9 where the critical load is applied. Since only the magnitude of the bridging stress and not the bridging mechanism is changed during cyclic fatigue it is reasonable to assume that the softening index, n, is maintained constant. Thus, both $\omega_c(N)$ and $G_f(N)$ are reduced proportionally with the frictional degradation and the $G_f(N)/\omega_c(N)$ ratio is maintained constant, i.e.

$$\frac{G_f(N)}{\omega_c(N)} = \frac{G_f}{\omega_c} \tag{17}$$

A similar constant G_f/ω_c ratio assumption has also been used to study the fracture process zone width variation in cementitious materials and the size effect in G_f [20, 35]. With Equation 17, the variation in $C_u(N)$ or the $\phi(N)$ function after fatigue cycle N is directly related to the diminution of the bridging zone, X.

Let N_c be the critical number of fatigue cycles at which the saturated bridging zone is completely destroyed due to the frictional degradation (in order to destroy all the bridges without causing crack growth the maximum load in the cyclic fatigue experiments has to be continually decreased. This problem is further discussed in Reference 24). Thus, if $N = N_c$, $X(N) = 0$ and $C_u(N) = C(a)$. Obviously, if $N = 0$, $X(N) = X$. Let $\Delta\phi(N) = \phi(a) - \phi(N)$, given by Equations 10 and 16

$$\begin{aligned}\Delta\phi(N) &= \phi(a) - \phi(N) \\ &= \frac{C^2(a)}{C'(a)}\left\{\frac{1}{C_u} - \frac{1}{C_u(N)}\right\} \\ &= \begin{cases} \frac{X - X(N)}{n+1} & N < N_c \\ \frac{X}{n+1} & N > N_c \end{cases} \end{aligned} \tag{18}$$

Comparing Equations 10 and 18, it is clear that $\Delta\phi(N)$ and $\phi(a)$ are similar curves having the same plateau of $X/(n+1)$ after $\Delta a > X$ or $N > N_c$.

The length of the bridging zone, $X(N)$, during cyclic fatigue can be determined from either Equation 16 or 18, i.e.

$$\begin{aligned} X(N) &= (n+1)\phi(N) \\ &= X - (n+1)\Delta\phi(N) \end{aligned} \tag{19}$$

The critical crack opening $\omega_c(N)$ during cyclic fatigue is given by

$$\begin{aligned}\omega_c(N) &= \frac{\omega_c}{X} X(N) \\ &= \omega_c \frac{(n+1)}{X}\phi(N) \\ &= \omega_c\left[1 - \frac{(n+1)}{X}\Delta\phi(N)\right] \end{aligned} \tag{20}$$

and the corresponding bridging stress distribution during cyclic fatigue is given by

$$\sigma_b(N) = \sigma_m\left[1 - \frac{\omega}{\omega_c(N)}\right]^n \tag{21}$$

The variations in σ_b and ω_c during fatigue is illustrated in Fig. 9 for the condition that the main crack a is about to grow.

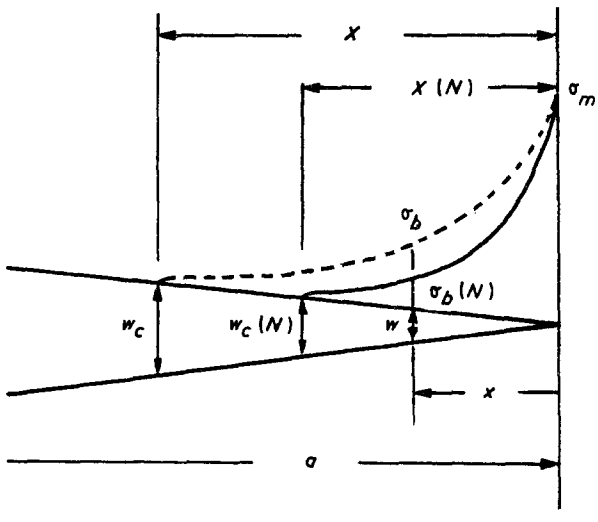

Figure 9 Variation in crack-interface bridging stresses due to frictional degradation of bridges during cyclic fatigue.

6. Conclusions

A new compliance ϕ function considering the influence of crack-interface bridging stresses has been defined by Equation 10 in this paper, from which a ϕ curve can be constructed easily in experiment. The ϕ function has a rigorous physical and mathematical basis, extended from the compliance and bridging stress theory [13, 20, 21]. Two ϕ curves can be obtained from compliance measurements: $\phi(a)$ with no sawcutting and $\phi(x)$ with consecutive sawcutting. Their respective derivatives defined in Equations 12 and 14 give the simplest expressions for the bridging stress in terms of compliance. Experimental results obtained from a range of engineering materials show that both the K_R (or G_R) and ϕ curves of a given material have similar features and the length of a fully saturated bridging zone can be determined equally well from both curves. The physics behind the relationship between the K_R and ϕ curves will be further investigated in detail in a separate paper [36].

From a ϕ curve measured in experiment the non-dimensional bridging stress distribution defined by Equation 6 can be readily determined with Equation 10. This new method for the determination of bridging stresses is much simpler than the consecutive sawcut technique if the precise bridging stress distribution is not required. The results collected in this paper suggest that the method is applicable to a wide range of brittle materials and fibre composites for which the main toughening mechanism is due to crack-interface bridging.

The potential of the ϕ curve to estimate the relative influences of crack-interface bridging and microcracking and to distinguish the so-called end effect associated with R curve measurements when a crack is close to the backface of a specimen warrants further investigation. In addition the use of the ϕ curve to study frictional degradation in bridges behind a crack tip due to cyclically applied loads should be examined.

Acknowledgements

The authors wish to thank the Australian Research Council (ARC) for the award of a National Research Fellowship to one of us (XH) and the continuing financial support of the project: "Development of High Strength-High Toughness Fibre Composites". Part of this work was performed by X. Hu on a Postdoctoral Fellowship at ETH, Institute for Building Materials, Zurich, Switzerland. Thanks are also due to S. Lathabai and E. H. Lutz for kindly providing details of their experimental results on alumina and duplex ceramics.

References

1. A. G. ATKINS and Y. W. MAI, in "Elastic and plastic fracture in metals, polymer, ceramics, composites, biological materials" (Ellis Horwood, 1985) pp. 817.
2. Y. W. MAI, *Mater. Forum*, **11** (1988) 232.
3. *Idem*, in Proceedings of NATO ARW on Toughening Mechanisms in Quasi-Brittle Materials, edited by S. P. Shah (1990) p. 489.
4. B. COTTERELL and Y. W. MAI, *Mater. Forum*, **11** (1988) 341.
5. Y. W. MAI and M. I. HAKEEM, *J. Mater. Sci.* **19** (1984) 501.
6. X. N. HUANG and D. HULL, *Comp. Sci. Technol.* **35** (1989) 283.
7. S. HASHEMI, A. J. KINLOCH and J. G. WILLIAMS, *Ibid.* **37** (1990) 429.
8. R. KNEHANS and R. W. STEINBRECH, *J. Mater. Sci. Lett.* **1** (1982) 327.
9. M. V. SWAIN, *ibid.* **5** (1986) 1313.
10. Y. W. MAI and B. R. LAWN, *J. Amer. Ceram. Soc.* **70** (1987) 289.
11. A. HILLERBORG, in "Fracture Mechanics of Concrete", edited by F. H. Wittmann (Elsevier, Amsterdam, 1983) p. 223.
12. R. M. L. FOOTE, Y. W. MAI and B. COTTERELL, *J. Mech. Phys. Solids*, **34** (1986) 593.
13. X. Z. HU and F. H. WITTMANN, in "Fracture of Concrete and Rock: Recent Developments", edited by S. P. Shah, S. E. Swartz and B. Barr (Elsevier, UK, 1989) p. 307.
14. V. S. GOPALARATNAM and S. P. SHAH, *J. Amer. Concr. Inst.* **82** (1985) 310.
15. P. E. PETERSSON, PhD Thesis, Lund Institute of Technology, Sweden (1981).
16. V. C. LI, in "Application of Fracture Mechanics to Cementitious Composites", edited by S. P. Shah (Martinus Nijhoff, Dordrecht, 1985) p. 431.
17. T. J. CHUANG and Y. W. MAI, *Int. J. Solids Structures*, **25** (1989) 1427.
18. Y. UCHIDA, K. ROKUGO and W. KOYANAGI, in Proceedings of Fracture Behaviour and Design of Materials and Structures, edited by D. Firras, Vol. 2 (Torino, 1990) p. 632.
19. X. Z. HU and F. H. WITTMANN, *J. Mater. Civil Engng.* **2** (1990) 15.
20. X. Z. HU, Postdoctoral Research Report, Swiss Federal Institute of Technology, Switzerland (1989).
21. X. Z. HU and F. H. WITTMANN, "An analytical method to determine the bridging stress transferred within the fracture process zone", to be published in Cement and Concrete Research (1991).
22. A. M. ALVAREDO, X. Z. HU and F. H. WITTMANN, in "Fracture of Concrete and Rock", edited by S. P. Shah, S. E. Swartz and B. Barr, (Elsevier, UK, 1989), p. 51.
23. X. Z. HU and Y. W. MAI, "Mode-I delamination and fibre-bridging in carbon-fibre/epoxy composites with and without PVAL coating" *Comp. Sci. & Techn*, in press.
24. X. Z. HU, Y. W. MAI and S. LATHABAI, "Compliance analysis of a bridged crack under monotonic and cyclic loading", *J. European Ceram. Soc.* 1991, in press.
25. H. E . LUTZ, PhD Thesis, Hamburg-Harburg University, Germany (1989).
26. E. H. LUTZ, N. CLAUSSEN and M. V. SWAIN, *J. Amer. Ceram. Soc.* **74** (1991) 11.
27. P. L. SWANSON, C. J. FAIRBANKS, B. R. LAWN, Y. W. MAI and B. J. HOCKEY, *J. Amer. Ceram. Soc.* **70** (1987) 279.
28. S. LATHABAI, J. RODEL and B. LAWN, *J. Mater. Sci.*, in press.
29. H. E. LUTZ and N. CLAUSSEN, *J. Euro. Ceram. Soc.* **7** (1991) 209, 219.
30. X. Z. HU, E. H. LUTZ and M. V. SWAIN, *J. Amer. Ceram. Soc.* **74** (1991) 1828
31. R. W. STEINBRECH, A. REICHL and W. SCHAARWACHTER, *J. Amer. Ceram. Soc.* **73** (1990) 2009.
32. J. K. KIM and Y. W. MAI, *J. Mater. Sci.* **26** (1991) 4702.
33. *Idem*, in Proceedings of the 2nd Australian SAMPE Symposium Exhibition, Melbourne (1989) p. 106.
34. J. RODEL, J. F. KELLY and B. R. LAWN, *J. Amer. Ceram. Soc.* **73** (1990) 3313.
35. X. Z. HU and F. H. WITTMANN, *Mater. and Struct.*, in press.
36. X. Z. HU, "*R*-curve and compliance ϕ-function for crack-interface bridging stress analysis", to be published.

Received 20 February
and accepted 20 June 1991